

Thermodynamic and economic analysis of a novel solar heating crude oil system in oil refinery

Yang Li¹, Jin-Rong Yang¹, Hong-Wei Chen¹ , Chang-Hua Lin²

¹ Liaoning Petrochemical University, College of Petroleum Engineering. Fushun, 113001, Liaoning, China.

²Qiandongnan Polytechnic College. Kaili City, 556099, Guizhou, China.

e-mail: chenhongwei@lnpu.edu.cn, liyang@lnpu.edu.cn, 13238582547@163.com, chenhongwei@lnpu.edu.cn, linchanghua0626@163.com

ABSTRACT

This study presents an innovative crude oil heating technology by introducing environmentally friendly solar energy into the petroleum industry. By integrating novel combination methods into traditional crude oil heating systems, a versatile and efficient crude oil heating system has been formed. The system was implemented in a refinery and its thermodynamic and economic performance was analyzed. The thermodynamic analysis, employing the exergy analysis method, reveals that among the considered parameters, compressor pressure ratio and Rankine cycle fluid flow rate exert the most significant influence on system efficiency. Overall, the system achieves energy efficiency, exergy efficiency, and waste heat recovery efficiency of 75.99%, 74.13%, and 31.21%, respectively. Within the system, solar collectors, TES tank, and compressor exhibit the highest exergy destruction rates, while pumps demonstrate the lowest exergy destruction rate. The economic analysis, using the annualized cost method, revealed that electricity prices have a significant impact on the economic performance of the system. The variation in system economic parameters is related to the annualized operating cost of the system. The system generates a net annual benefit of 0.591 million US\$, with a 4.124-year investment return period. Moreover, Sensitivity analysis explores various factors affecting the crude oil heating system's performance.

Keywords: Heating crude oil; Solar energy; Energy analysis; Exergy analysis; Economic analysis.

1. INTRODUCTION

At present, global attention is focused on energy and environmental issues, the use of fossil fuels as primary energy sources has led to significant environmental hazards. The interconnected problems of climate warming, atmospheric pollution, and energy shortages have emerged [1]. Worldwide, countries are actively pursuing the path of sustainable development, seeking a harmonious balance between humanity and nature. According to projections from the International Energy Agency [2], the consumption of primary energy is expected to progressively rise until 2050, with an average annual increase of 3% from 2018 to 2050, which is the result of the role of renewable energy. Solar energy, among various renewable energy sources, is widely utilized in diverse fields due to its universality, accessibility, and abundant reserves. Applications include crude oil heating [3], photovoltaic power generation [4], solar-powered buildings [5], and seawater desalination [6]. Integrating solar energy with the storage and transportation of crude oil is a crucial approach to reducing energy consumption and environmental pollution. A better understanding of solar heating technology for crude oil is strongly needed.

Heavy crude oil extraction, transportation, and processing necessitate significant direct or indirect heat consumption, resulting in the emission of a substantial amount of carbon dioxide. WANG *et al.* [7] evaluated the potential utilization of solar energy in the global oil operations industry. Among them, the demand for solar photovoltaic and solar thermal in the refining industry ranges from 17 to 95 GW and 21 to 95 GW, respectively, which indicates that solar energy is playing an increasingly important role in the oil and gas industry. ALIREZA *et al.* [8] combined gas and steam turbine cycles with an ORC-VCR system to achieve a highly efficient layout from technical, economic, and environmental perspectives. RAVINDER *et al.* [9] described the economic and thermal performance of a 210 MW coal-fired power station. Equipment cost, fuel cost, operation and maintenance expenses, income, and the net present value of the plant are all analyzed as part of the economic analysis. By 2035, solar energy is expected to contribute approximately 2 trillion joules of energy, constituting around 5% of the industry's overall energy demand [10]. Relevant statistics reveal that at least 20% of energy consumption

Table 1: Structural parameters of TES tank.

PARAMETER	VALUE
Material	Mullite-Cordierite
Hole pattern	Hexagonal hole
Aperture	2.9 mm
Wall thickness	0.8 mm
Porosity	0.61
Density	958 kg/m ³
Specific heat capacity	1000 J/(kgK)
Diameter	1.5 m
Height	4 m

acquisition and high thermal efficiency. The outlet temperature of the HTF is contingent on the size and number of collectors, and this study assumes a solar radiation of 900 W/m² [19]. Due to the small impact of pressure drop on system parameters, it can be disregarded. The flow rate of the HTF is taken as 40 kg/s. The thermal energy storage tank is composed of honeycomb ceramic material, with its structural parameters presented in Table 1. Honeycomb ceramic materials are capable of withstanding high temperature and possess low thermal inertia. Its ordered porous structure determines low flow resistance, a large specific surface area and is widely used as an energy storage material for high temperature air. In the honeycomb ceramic thermal energy storage tank, the hot air flows through the tank during the charging period to store the heat and the temperature of the tank increases. When the heat is released, the cold air flows through the same channel to absorb the previously stored heat, and the temperature of the tank subsequently decreased. The heat of the tank comes from the hot air of the solar field. When there is no sunlight, the TES tank is utilized to heat the crude oil while generating electricity through the Rankine cycle. The system can be heated directly by solar energy during the day and indirectly by the TES tank at night.

The ceramic material, selected silicon carbide, can operate at a temperature between 1000 °C and 2000 °C, which is consistent with the working temperature of the dish solar collector, so the use of this material is the correct choice. The average sunshine duration in this work is 10 hours per day, which is also the charging period of the TES tank. After sunset, the tank is used for heating. It has a discharging period of 8 hours, and one hour of heat storage time is considered before the discharging period.

The crude oil heating system includes a traditional oil heater and a proposed solar heating system. The physical and chemical properties of different types of crude oil can significantly affect their heating effectiveness. In the crude oil production process, it is essential to select suitable heating methods and conditions based on the specific type and properties of the crude oil to achieve optimal heating results. Using the solar system, the crude oil is heated from 25 °C at point 1 to 320 °C at point 10, which is also the main energy input considered in this work, and then continued to heat the crude oil to 380 °C using conventional heaters. The crude oil heating system includes three shell and tube heat exchangers to transfer the heat of the air to the crude oil. The solar energy effectively reduces the load on the conventional fired heater by heating the crude oil to 320 °C. In addition, crude oil contains salts that are harmful to downstream equipment and must be removed. Therefore, considering the desalination stage, the desalter is located between the first and second heat exchangers. The salty crude oil enters at point 3 and exits at point 6 with temperature of 120 °C and 110 °C, respectively. After the desalted crude oil leaves the second heat exchanger, it enters the flash tank at point 7 to remove the volatile light hydrocarbon components from the crude oil. The crude oil is separated in the flash tank into pre-flashed crude gas and pre-flashed crude liquid. The pre-flashed crude liquid at point 8 enters a third heat exchanger for further heating, followed by the conventional fired heater.

3. SYSTEM MODELING AND SIMULATION

3.1. Simulation conditions

Aspen Plus, as a large-scale general process simulation software, has a complete physical property system, so this software is used for simulation in this study. The relevant physical properties of the crude oil are inputted

Table 2: Simulation conditions of the proposed system.

PARAMETER	VALUE
Ambient temperature	25 °C
Ambient pressure	101.3 kPa
The minimum heat exchange temperature difference of the heat exchanger	15 °C
The isentropic efficiency of the pump and compressor	85%
The flow rate of crude oil	14 kg/s
The flow rate of air	40 kg/s
The initial temperature of air	20 °C
The initial temperature of crude oil	25 °C
The final temperature of crude oil	320 °C

into the software based on its molecular composition. Within this software, the physical property methods suitable for crude oil distillation encompass K-value models such as BK10, Grayson, Chao-Sea, and equations of state adjusted for oil such as RK-Soave and Peng-Rob. Since the BK10 physical property method is suitable for reduced pressure and low pressure (up to several atmospheres), while the RK-Soave and Peng-Rob equations of state are more suitable for high-pressure conditions, the built-in BK10 physical property method is selected for simulation. Aspen Plus software provides a variety of convergence algorithms. Different modules require different convergence methods. The commonly used method is the WEGSTEIN method. This method is a direct iterative loop and can calculate multiple streams at the same time. It is generally regarded as the fastest and most reliable convergence algorithm, so this method is chosen as the convergence algorithm of this study. The simulation conditions of the proposed system are shown in Table 2.

- (1) Air is considered as an ideal gas.
- (2) Air is a binary mixture composed of N₂ and O₂, and the influence of water vapor, CO, and other substances in the air on the thermal process of the system is not considered.
- (3) The pressure loss of air flowing in the pipeline is not considered.
- (4) Cycle power consumption and pressure loss on the heat exchange working medium side are not considered.
- (5) Thermal losses only occur in the solar collector.
- (6) In the static simulation, the influence of time on the operating conditions is not considered.

3.2. Thermodynamic model

3.2.1 Modeling of the solar collector subsystem

Assuming the DNI is constant, and the system is in a steady state. The power of the solar radiation reaching the surface of the dish collector is calculated using the following equation [20]:

$$Q_s = I_s A_a \quad (1)$$

where Q_s is the power of solar energy reaching the surface of the dish collector (W). I_s is the solar radiation intensity reaching the surface of the collector (W/m²). A_a is the surface area of the collector (m²).

When the system is in steady condition, the useful energy delivered by the solar collector system is equal to the energy absorbed by the HTF, which is determined by the radiant solar energy falling on the receiver minus the direct or indirect heat loss from the receiver to the surrounding environment, that is:

$$Q_u = Q_r - Q_l \quad (2)$$

where Q_u is the useful power reaching the receiver (W). Q_r is the power reflected by the collector to the receiver (W). Q_l is the power lost in the receiver (W).

The optical efficiency (η_{opt}) of the solar receiver is defined as the ratio of the power reaching the receiver (Q_r) to the power from the sun (Q_s). The thermal efficiency (η_r) of the solar receiver is defined as the ratio of useful power (Q_u) reaching the receiver to the power reaching the receiver (Q_r). The thermal efficiency of the collector (η_c) is defined as the ratio of the useful power (Q_u) reaching the receiver to the power (Q_s) from the sun, that is [20]:

$$\eta_{opt} = \frac{Q_r}{Q_s} \quad (3)$$

$$\eta_r = \frac{Q_u}{Q_r} \quad (4)$$

$$\eta_c = \frac{Q_u}{Q_s} \quad (5)$$

Combined with Equations (2)–(5), the thermal efficiency of the collector can be written as:

$$\eta_c = \eta_{opt} - \frac{Q_l}{Q_s} \quad (6)$$

The optical efficiency (η_{opt}) of the solar receiver depends on the optical properties of the selected materials and the geometry of the receiver, etc. An approximate analysis of optical efficiency can be performed using the following equation:

$$\eta_c = \rho\tau\alpha\gamma \left[(1 - A_f \tan \theta) \cos \theta \right] \quad (7)$$

where ρ , $\tau\alpha$, γ , A_f , θ are the reflectance of the mirror, transmittance-absorptance product, the absorptance of the receiver, the intercept factor, and the incident angle, respectively. The solar collector is equipped with a solar tracking system, the dish collector keeps tracking the sun along two axes when solar radiation is available, so the incident angle θ is 0 ($\tan \theta = 0$, $\cos \theta = 1$), Equation (7) can be written as:

$$\eta_c = \rho\tau\alpha\gamma \quad (8)$$

The power loss in the receiver mainly consists of three parts: (a) the heat conduction loss of the receiver, Q_{lk} . (b) the convective heat transfer loss through the receiver aperture, Q_{lc} . (c) the radiant heat loss through the receiver aperture, Q_{lr} . The total heat loss of the receiver can be expressed as:

$$Q_l = Q_{lk} + Q_{lc} + Q_{lr} \quad (9)$$

In this work, the impact of wind is ignored. A transparent window is installed at the opening of the receiver to block the dust in the air, which can prevent forced convection to a certain extent, so the real convection is the main heat loss [21]. The power of convective heat transfer loss (Q_{lc}) is:

$$Q_{lc} = h_c A_w (T_w - T_a) \quad (10)$$

where T_w , T_a , and A_w are the temperature of the receiver (K), the ambient temperature (K), and the internal area of the receiver cavity (m^2), respectively. h_c is the convective heat transfer coefficient between the receiver and the environment ($\text{W}/(\text{m}^2\text{K})$).

Since the receiver inlet aperture area is smaller compared to the inner cavity area, this results in smaller radiation losses. The inlet aperture area is related to the geometric concentration ratio, which is defined as the ratio of the aperture area of the dish collector to the inlet aperture area of the receiver. The power of the receiver through radiation heat transfer loss (Q_{lr}) can be estimated using the following equation [21]:

$$Q_{lr} = A_c \varepsilon_{ff} \sigma (T_w^4 - T_a^4) \quad (11)$$

$$A_c = A_a / C \quad (12)$$

$$\varepsilon_{eff} = 1 / [1 + (1 / \varepsilon_c - 1) A_c / A_w] \quad (13)$$

where A_c is the aperture surface area (m^2) of the receiver. C is the geometric concentration ratio. ε_{eff} is the effective infrared emittance of the cavity. ε_c is the surface emittance of the cavity. σ is the Stefan-Boltzmann constant.

In actual operation, the outer surface of the receiver is usually covered with a thick opaque insulating layer to reduce thermal conduction loss. Studies have shown that thermal conduction loss is usually insignificant compared to convection and radiation loss. Therefore, in this work, it is assumed that the outer wall of the receiver is adiabatic, meaning the heat conduction loss of the receiver is $Q_{ik} = 0$.

3.2.2. Exergy analysis model

The method of exergy analysis is used to analyze the system in detail. Exergy analysis considers the factors such as effective energy and thermodynamic irreversibility and can identify the primary exergy loss process in the system. The mathematical models of each part are as follows:

The system is in a stable operating condition, and its mass balance equation is [7]:

$$\sum m_{in} = \sum m_{out} \quad (14)$$

where m is the mass flow rate (kg/s). the energy equation of the system is:

$$Q - W = \sum m_{out} h_{out} - \sum m_{in} h_{in} \quad (15)$$

where Q is the heat transfer rate (kW), W is the work generation rate (kW), h is the specific enthalpy (kJ/kg).

The exergy balance equation can be expressed as:

$$\sum Ex_{in} = \sum Ex_{out} + Ex_d \quad (16)$$

$$\sum m_{in} ex_{in} + Ex_Q = \sum m_{out} + ex_{out} + Ex_W + Ex_d \quad (17)$$

where Ex is the exergy rate (kW), Ex_Q and Ex_W are the exergy rates related to heat transfer and work, respectively (kW). Ex_d is the exergy destruction rate (kW), ex is the specific exergy (kJ/kg). The exergy related to the heat transfer rate can be expressed as:

$$Ex_Q = \left(1 - \frac{T_0}{T_s}\right) Q \quad (18)$$

where T_0 is the ambient temperature (K), T_s is the source temperature (K). Furthermore, the exergy associated with the work interaction can be expressed as:

$$Ex_W = W \quad (19)$$

The physical exergy of each state point [22]:

$$ex_i = h_i - h_0 - T_0 (s_i - s_0) \quad (20)$$

where s is the specific entropy (kJ/(kg·K)). For a defined energy system, the main steps in performance evaluation include determining the exergy destruction rates. The exergy destruction rate of the system can be expressed as:

$$Ex_d = T_0 S_{gen} \quad (21)$$

where T_0 is the reference temperature (K), S_{gen} is the entropy generation rate of the given process (kJ/(s·K)). Since crude oil is an incompressible substance, it can be expressed by the following entropy change equation:

$$s_2 - s_1 = C_{p,avg} \ln \frac{T_2}{T_1} \quad (22)$$

where $C_{p,avg}$ is the specific heat of crude oil, which can be calculated by the following correlation formula:

$$C_{p,avg} = 1940 + 3T \quad (23)$$

where T is the average temperature of each process (°C).

The energy balance equation of the TES tank k is:

$$\sum m_{in} h_{in} t + \dot{m}_{tank} u_i + \sum Q_{in} t = \sum m_{out} h_{out} t + \dot{m}_{tank} u_f + \sum Q_{out} t \quad (24)$$

where t is time (s), m is the mass of the TES tank k (kg), u_i and u_f are the initial and final internal energy, respectively (kJ/kg).

Entropy is created in a process due to the existence of irreversibility, which can be assessed by applying the entropy equilibrium equation:

$$\sum m_{in} s_{in} t + \dot{m}_{tank} s_i + \sum \frac{Q_{in}}{T} t + S_{gen} = \sum m_{out} s_{out} t + \dot{m}_{tank} s_f + \sum \frac{Q_{out}}{T} t \quad (25)$$

The exergy balance equation of the TES tank k can be expressed as:

$$\sum m_{in} ex_{in} t + \dot{m}_{tank} ex_i + \sum Ex_{in}^Q = \sum m_{out} ex_{out} t + \dot{m}_{tank} ex_f + \sum Ex_{out}^Q \quad (26)$$

In addition, the storage capacity of TES tank can be calculated by the following formula:

$$\dot{Q} = C_p \rho_s (1 - \varepsilon) \cdot V_{tank} \cdot (T - T_0) \quad (27)$$

where C_p is the specific heat capacity of the porous medium (J/(kg·K)), ρ_s is the density of the matrix material of the porous medium (kg/m³), ε is the porosity, V_{tank} is the volume of the TES tank k (m³), T is the temperature of the TES tank k at a certain time (K); T_0 is the initial temperature of the TES tank k (K).

The performance of the system can be evaluated in terms of energy and exergy efficiency. The energy efficiency of thermal energy storage can be defined by the following equation:

$$\eta_{en_{TES}} = \frac{Q_{discharging}}{Q_{charging}} = 1 - \frac{Q_{losses}}{Q_{charging}} \quad (28)$$

The overall energy efficiency of the proposed system is shown below:

$$\eta_{en_{overall}} = \frac{W_{net_{system}} + Q_{oil}}{Q_{solar}} \quad (29)$$

where Q_{solar} represents the solar energy input to the system (kW), $W_{net_{system}}$ represents the net output work of the integrated system (kW). In this system, the following formula can be used to calculate:

$$W_{net_{system}} = W_{turbine} + W_{compressor} - \sum W_{pumps} \quad (30)$$

The parameter Q_{oil} represents the heat gain of the crude oil (kW). The following formula can be used to calculate [7]:

$$Q_{oil} = m(h_{10} - h_2) \quad (31)$$

The exergy efficiency of any given process is defined as the ratio of the exergy output to the exergy input. The exergy efficiency of the solar energy and the system can be calculated as follows:

$$\eta_{ex_{solar}} = 1 - \frac{Ex_{d_{solar}}}{Q_{solar} \left(1 - \frac{T_0}{T_{sun}} \right)} \quad (32)$$

$$\eta_{ex_{overall}} = \frac{W_{net_{system}} + Q_{oil} \left(1 - \frac{T_0}{T_{oil_{avg}}} \right)}{Q_{solar} \left(1 - \frac{T_0}{T_{sun}} \right)} \quad (33)$$

After the air heats the crude oil and generates electricity, it enters the preheater to preheat the cold air, and the air coming out of the preheater also has a certain amount of heat. Its value in the total input energy of the system is the system waste heat recovery efficiency η_w .

$$\eta_w = \frac{Q_w}{Q_s} \quad (34)$$

3.2.3. Validation

In this work, to evaluate the thermal performance of the dish-type collector, an approximate estimation of the optical efficiency is made, and the emphasis is placed on the calculation of thermal efficiency in the receiver. The temperature range selected for the receiver research is 800 °C to 1300 °C to validate the analytical model established in Section 3.2. Other relevant information required can be found in Table 3 [20].

The comparison results are shown in Table 4. It can be observed from the table that the results of this work are less different from the results in the reference. The error range is only between 0.03% and 0.12%.

3.3. Economic model

The economic analysis of the system is carried out using annualized cost. In this method, all the costs of the system are calculated over its estimated life. The costs include annualized capital cost (C_{acap}), annualized replacement

Table 3: The main parameters of the solar concentrating system [20].

PARAMETER	SYMBOL	VALUE
Dish concentrator aperture area	A_a	11×11 m ²
Normal direct insolation (DNI) per unit of collector area	I_s	900 W/m ²
Reflectivity of dish surface	ρ	0.94
Transmittance–absorptance product	$\tau\alpha$	0.99
Intercept factor of receiver	γ	0.99
Cavity internal area of the receiver	A_w	0.0654 m ²
Radiative emissivity of cavity	ε_c	0.9
Geometrical concentration ratio	C	3000
Stefan–Boltzmann constant	σ	5.672 × 10 ⁻⁸ W/(m ² K ⁴)
Ambient temperature	T_a	25 °C

Table 4: Validation of the thermal efficiency of the solar receiver in various average operating wall temperature in the cavity.

AVERAGE WALL TEMPERATURE IN THE CAVITY (°C)	THERMAL EFFICIENCY (%)		
	THIS WORK	REF. [20]	ERROR
800	96.65	96.62	0.03
850	96.12	96.08	0.04
900	95.52	95.47	0.05
950	94.84	94.79	0.05
1000	94.08	94.03	0.05
1050	93.25	93.18	0.07
1100	92.31	92.24	0.07
1150	91.29	91.20	0.09
1200	90.14	90.04	0.10
1250	88.88	88.77	0.11
1300	87.50	87.38	0.12

Table 5: Purchased cost of components.

COMPONENT	PURCHASED EQUIPMENT COST FUNCTIONS	REFERENCE
Heat exchanger	$C_{HX} = 8500 + 409N_{HX}^{0.85}$	[22]
Pump	$C_{pump} = 705.48\dot{W}^{0.71} \left(1 + \frac{0.2}{1 - \eta_{pump}} \right)$	[23]
Collector	$C_{CSP} = 50N_{CSP}$	[21]
Compressor	$C_{compressor} = \frac{39.5 \times \dot{m}}{\varepsilon_C} \left(\frac{p_{dc}}{p_{suc}} \right) \ln \left(\frac{p_{dc}}{p_{suc}} \right)$	[24]
Turbine	$C_{turbine} = 3644.3\dot{W}^{0.7} - 61.3\dot{W}^{0.95}$	[22]
Boiler	$C_{boiler} = (0.249p_{boiler} + 47.19)\dot{m} + 3.29p_{boiler} + 624.6$	[25]
Condenser	$C_{condenser} = 516.621N_{condenser} + 268.45$	[22]
TES tank	$C_{storage} = 17400 + 79W_{storage}^{0.85}$	[26]
Desalter	$C_{desalter} = 8500 + 409N_{desalter}^{0.85}$	[22]
Flash drum	$C_{drum} = 1.218f_m \exp[9.1 - 0.2889 \ln w + 0.04576(\ln w)^2] + 300D^{0.7396}L^{0.7066}$ $f_m = 0.0172, W = 10000, D = 8, L = 15$	[23]
Generator	$C_{generator} = 60\dot{W}^{0.95}$	[27]
Preheater	$C_{PRE} = 8500 + 409N_{PRE}^{0.85}$	[22]

cost (C_{arep}), annualized maintenance cost (C_{amain}) and annualized operating costs (C_{aope}). It is assumed that the annual inflation rate and the annual real interest rate are equal to 17% and 20%, respectively, with a project life cycle of 20 years. Tables 5 and 6 show the cost functions of the components and the process of economic analysis of the system, respectively.

4. RESULTS AND DISCUSSION

According to the mathematical model established above, some useful results are obtained through calculation. The overall energy efficiency, exergy efficiency, and waste heat recovery efficiency of the system are 75.99%, 74.13%, and 31.21%, respectively. The net annual benefit, annualized operating cost, and return period of the system are 0.591 million US\$, 13.691 million US\$, and 4.124 years, respectively. A parametric study is

Table 6: Economic parameters in annualized cost of system.

DEFINITION	PARAMETER	REFERENCE
Annualized cost of system	$ACS = C_{acap} \text{ (Components)} + C_{arep} \text{ (Components)} + C_{amain} \text{ (Components)} + C_{aope} \text{ (Labor cost + Insurance cost + Fule cost)}$	[28]
Annualized capital cost	$C_{acap} = C_{cap} \cdot CRF(i, y) = C_{cap} \cdot \frac{i(1+i)^y}{(1+i)^y - 1}$ $C_{cap} = 1.1 \text{ of total capital cost; } i = \frac{z-n}{1+n}$	[29]
Annualized replacement cost	$C_{rep} = C_{cap} \text{ (in Base year)} \cdot (1+i)^y$ $C_{arep} = C_{rep} \cdot FSF(i, y) = C_{rep} \cdot \frac{i}{(1+i)^y - 1}$	[29]
Annualized maintenance cost	$C_{amain} = 0.05 \text{ of total capital cost}$	[28]
Annualized operating cost	$C_{aope} = \text{Labor cost} + \text{Insurance cost} + \text{Fule cost} + \text{Utility}$ Number of labor = 80, Labor cost = 500 US\$/month Fuel cost (Electrical energy price) = 0.15 US\$/kW·h Fuel cost (Water price) = 0.18 US\$/m ³ Insurance cost = 0.02 of capital cost	[29]
Net present value	$NPV = \frac{ACS}{CRF(i, y)}$	[25]
NEW ACS = ACS-I I = Solar power generation cost (US\$/year)	Produced electricity price: 0.15 US\$/kW·h	[23]
Levelized cost of product total product in one year (crude oil)	$LCP = \frac{NEW ACS}{\text{Annual output roudct of the system}}$	[29]
Prime cost	$VOP = \text{Volume of product}$ $PC = \frac{C_{aope}}{VOP}$	[23]
Summary of product cost	$COP = \text{Cost of product}$ $SPC = VOP \cdot COP$	[30]
Annual benefit	$AB = SPC - C_{aope}$	[23]
Net annual benefit	$NAB = AB \cdot (1 - \text{Tax percent}), \text{Tax} = 0.1(AB)$	[23]
Period of return	$PR = \frac{C_{cap}}{NAB}$	[23]
Rate of return	$RR = \frac{NAB}{C_{cap}}$	[23]
Additive value	$AV = COP - PC$	[23]

performed to analyze the effect of changing system parameters on its performance. For example, these system parameters include mass flow rate, turbine inlet temperature and pressure, compressor pressure ratio, and electricity price. The reference ambient temperature and pressure considered in this work are 25 °C and 101.3 kPa, respectively. Table 7 lists the data of each state point of the heating system.

Figure 2(a) shows the effect of different compressor pressure ratios on the energy efficiency and exergy efficiency of the system. As the pressure ratio increases, the energy efficiency from 44% to around 95%, and the exergy efficiency increased from 37% to around 96%. The reason for this trend is that when the pressure ratio increases, the air temperature at the compressor outlet also increases gradually, so when the maximum temperature of the solar collector is constant, the solar heat absorbed by it will decrease. Figure 2(b) shows the effect of the compressor pressure ratio on the net output work of the system. It can be observed that when the pressure ratio is increased from 2 to 7, the net output work of the system increases from 4563 kW to 13289 kW.

Table 7: Data of each state point of the heating system.

STATE NO.	STATE COMPOSITION	\dot{m} (kg/s)	T (°C)	P (kPa)	h (kJ/kg)	s (kJ/(kg·K))	ex (kJ/kg)
1	crude oil	14	25	100	-1990.86	-6.83	46.11
2	crude oil	14	25.67	150	-1990.77	-6.83	46.41
3	crude oil	14	120	150	-1761.84	-6.19	85.09
4	water	22	35	150	-15824.00	-8.92	-13162.49
5	water	22	38.91	150	-15807.70	-8.87	-13161.84
6	crude oil	14	110	150	-1787.46	-6.25	78.47
7	crude oil	14	210	150	-1516.43	-5.64	167.30
8	crude oil	13.12	200	958.27	-1575.83	-5.84	165.98
9	crude oil	0.88	200	958.29	-1676.40	-5.27	-104.87
10	crude oil	13.12	320	958.29	-1221.61	-5.19	326.79
11	air	40	25	100	-0.2219	0.0038	0
12	air	40	264.67	500	242.62	0.14	202.71
13	air	40	480.48	500	357.61	0.33	259.80
14	air	40	1000	500	1061.69	1.09	738.57
15	air	20	950	500	771.28	0.84	523.79
16	air	20	749.24	500	538.85	0.58	366.98
17	air	20	580.49	500	349.13	0.32	255.26
18	air	20	433.5	500	188.88	0.03	180.25
19	air	20	950	500	771.28	0.84	523.79
20	air	20	780.19	500	599.69	0.65	406.32
21	water	65	15	100	-15907.60	-9.2	-13162.58
22	water	65	25	100	-15868.90	-9.07	-13160.33
23	water	1	800	15000	-12391.60	-2.75	-11569.38
24	water	1	180.37	10	-13333.40	-1.12	-12999.16
25	water	1	30	10	-15845.00	-8.99	-13163.22
26	water	1	31.92	15000	-15823.5	-8.97	-13147.89
27	air	40	609.71	500	394.28	0.39	280.04
28	air	40	400	500	279.29	0.20	219.73

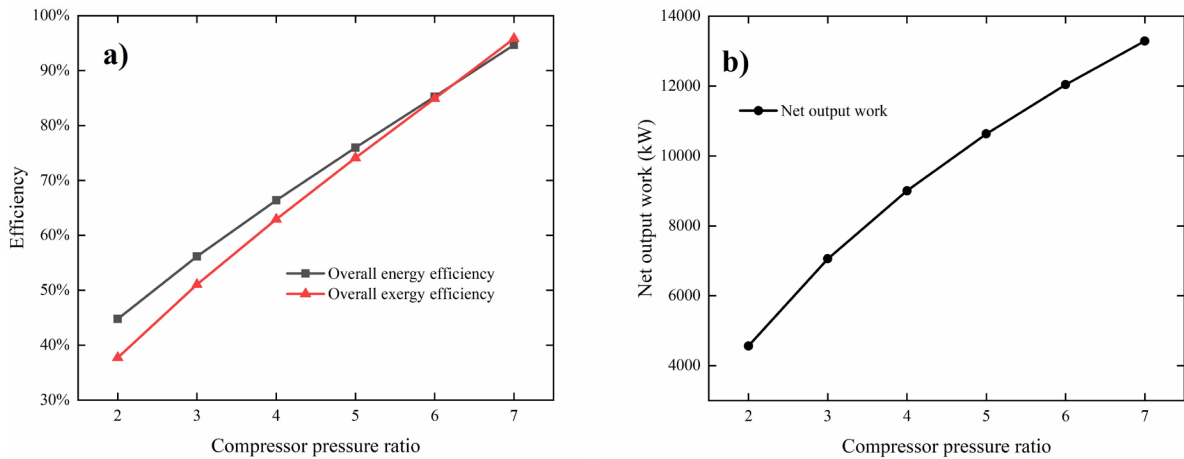


Figure 2: The effect of compressor pressure ratio on (a) overall energy efficiency and exergy efficiency, and (b) system net output work.

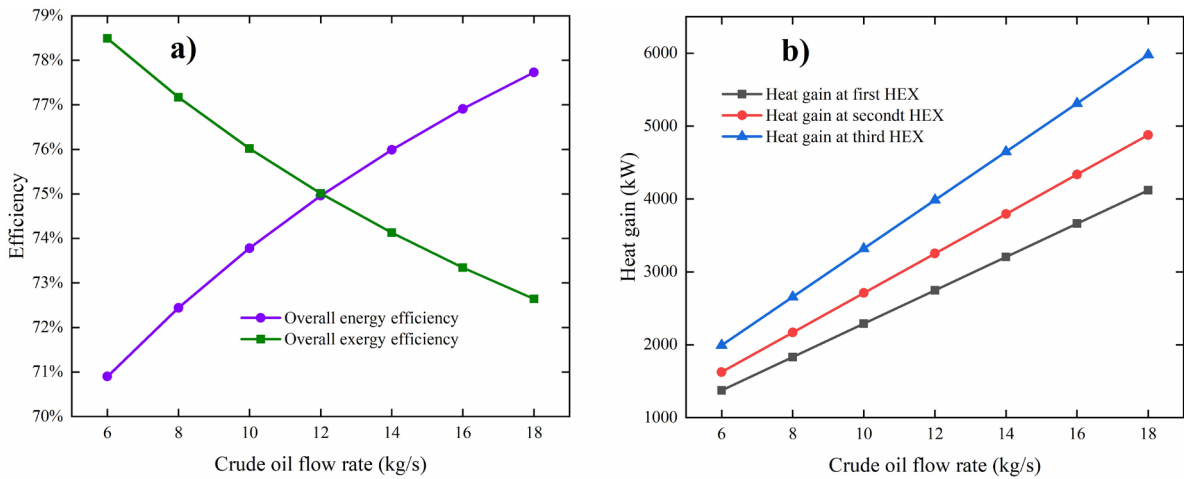


Figure 3: The effect of crude oil flow rate on (a) overall energy efficiency and exergy efficiency, and (b) heat gain of heat exchangers.

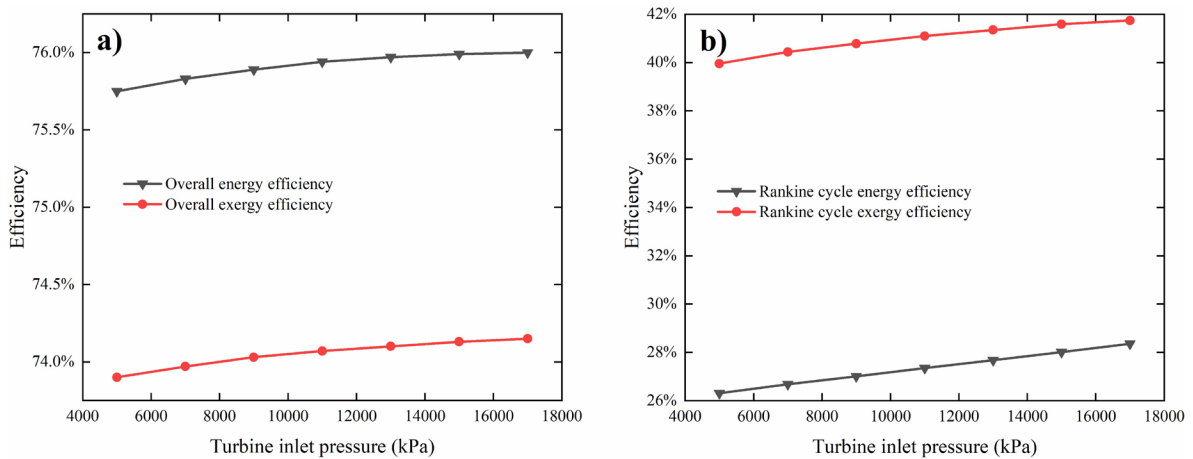


Figure 4: The effect of turbine inlet pressure on (a) overall energy efficiency and exergy efficiency, and (b) Rankine cycle energy efficiency and exergy efficiency.

Figure 3(a) shows the effect of crude oil flow rate on both overall energy efficiency and exergy efficiency. As the crude oil flow rate increases from 6 kg/s to 18 kg/s, the overall exergy efficiency decreases from 78.49% to 72.64%, while the energy efficiency increases from 70.90% to 77.73%. This is because, with an increase in crude oil flow rate, both the heat gain of crude oil and the solar energy required by the system also increase. For energy efficiency, the increase in heat gain is greater than the solar energy required by the system, while the exergy efficiency is the opposite, which also illustrates the importance of exergy in energy system analysis. As shown in Figure 3(b), the heat supplied to the heat exchangers increases significantly with the increase of the crude oil flow rate.

Another key system parameter that influences the system performance is the turbine inlet pressure, whose effect on the overall efficiency is depicted in Figure 4(a), and the inlet pressure varies from 5000 kPa to 17000 kPa. The efficiency of the system tends to increase as the inlet pressure increases. It is observed that the increase in inlet pressure eventually plateaus, and the system achieves its highest energy and exergy efficiency at a pressure of 15500 kPa. Furthermore, Figure 4(b) shows the effect of different turbine inlet pressures on the efficiency of the Rankine cycle. While the efficiency of the Rankine cycle increases with higher turbine inlet pressures, the magnitude of the increase is relatively modest. This can be attributed to the higher pumping work needed to reach these pressures. Moreover, the impact of changes in turbine inlet temperature on overall energy efficiency and exergy efficiency is depicted in Figure 5(a) and Figure 5(b), with the inlet temperature ranging from 525 °C to 725 °C. It can be observed that as the turbine inlet temperature increases, the exergy efficiency of the system increases, while the energy efficiency decreases. This is because the power consumption of the turbine increases with the

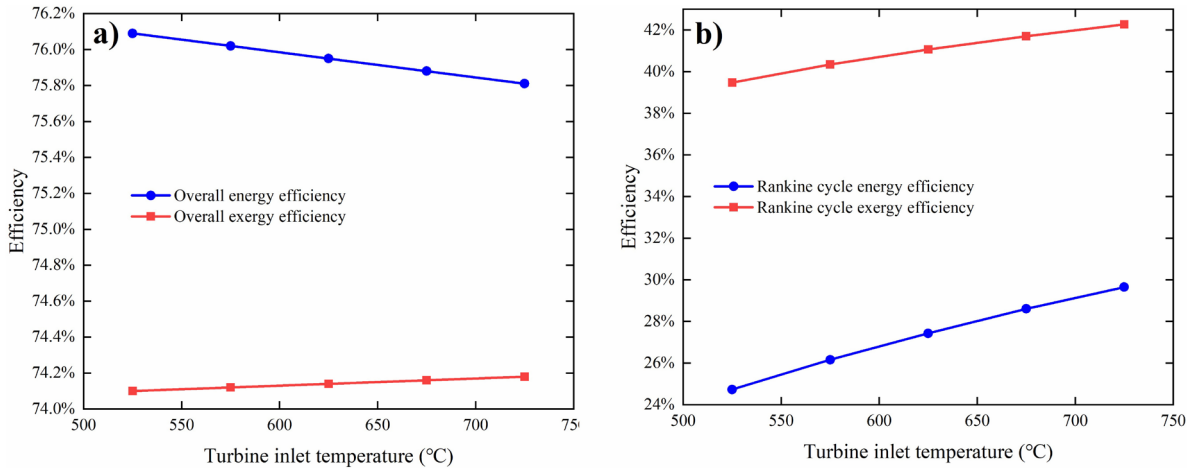


Figure 5: The effect of turbine inlet temperature on (a) overall energy efficiency and exergy efficiency (b) Rankine cycle energy efficiency and exergy efficiency.

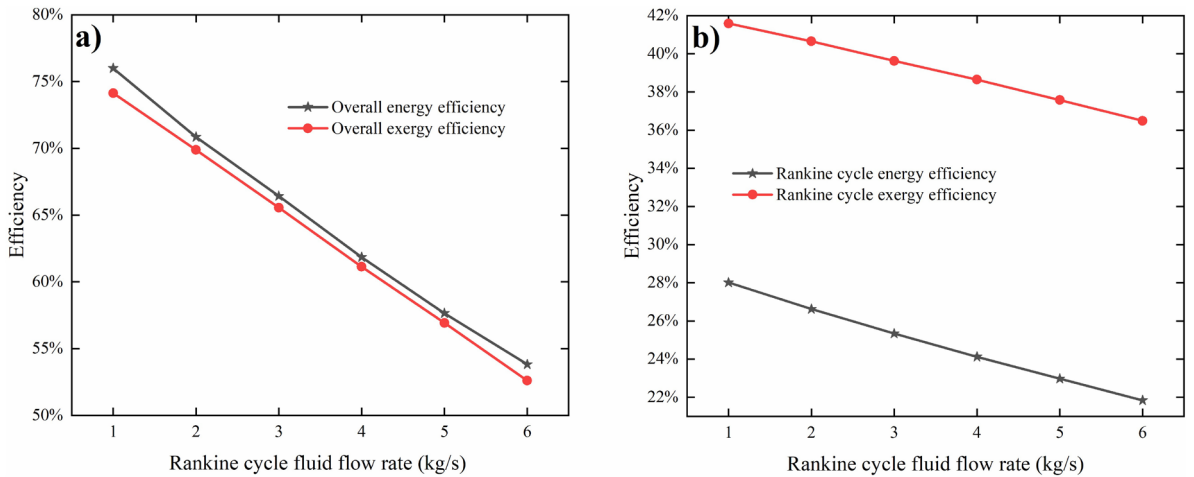


Figure 6: The effect of Rankine cycle fluid flow on (a) overall energy efficiency and exergy efficiency, and (b) Rankine cycle energy efficiency and exergy efficiency.

rise in inlet temperature, and the system needs to input more energy, but the power consumption of the compressor increases faster than the energy input to the system. As the turbine inlet temperature increases, so does the useful power output from the turbine, and therefore, an increase in the efficiency of the Rankine cycle is also observed.

Figure 6 shows the effect of the mass flow rate of the working fluid in the Rankine cycle on the overall efficiency as well as the efficiency of the Rankine cycle. It can be seen from the figure that with the increase of flow rate, the system efficiency and the efficiency of the Rankine cycle are constantly decreasing, which reduces the performance of the system. Therefore, the fluid flow rate of the Rankine cycle should be selected reasonably, not the higher the better. Through trial calculation, it is found that when the flow rate is 1 kg/s, the system performance is better, and this flow rate is selected as the optimal flow rate of the Rankine cycle in this work.

Furthermore, Figure 7(a) and Figure 7(b) illustrate the impact of charging and discharging duration on the energy and exergy efficiency of the TES tank. We define that the TES tank energy output refers to the energy recovered from the TES tank during discharge, while the TES tank energy input refers to the energy stored in the TES tank during charging and storage. This results in a downward trend in both energy efficiency and exergy efficiency during charging, with energy efficiency dropping from 64.58% to 48.43% and exergy efficiency dropping from 77.22% to 53.04%. Conversely, as the discharge duration increases, the energy recovered from the TES tank also increases. Therefore, the energy efficiency increased from 21.79% to 65.38%, and the exergy efficiency is raised from 34.98% to 79.02%. Furthermore, an increase in TES tank efficiency is observed as the discharge duration increased from 3 to 11 h, as shown in Figure 7(b). The linear variation in TES energy efficiency is attributed to the relative stability and

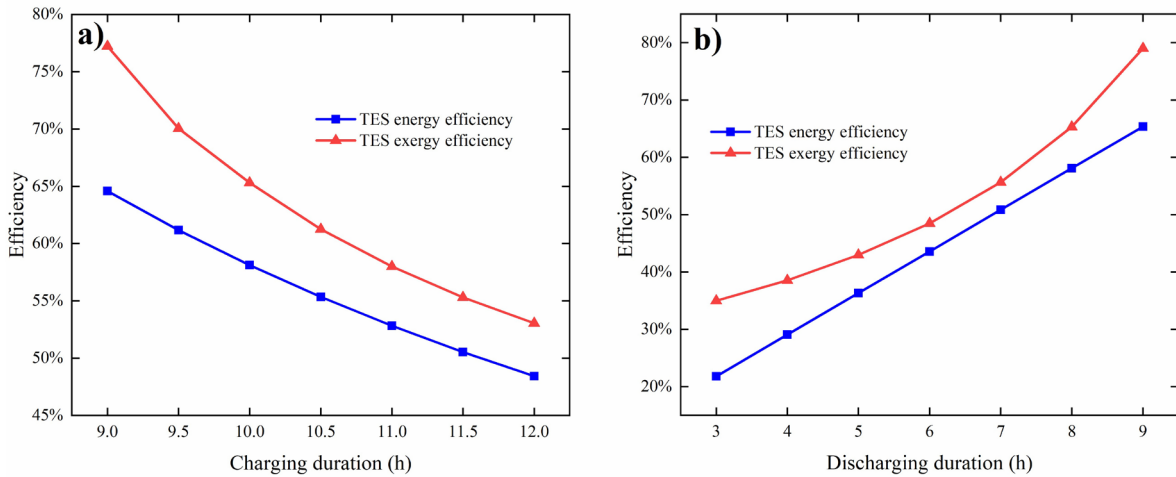


Figure 7: (a) The effect of charging duration on TES energy efficiency and exergy efficiency. (b) The effect of discharging duration on TES energy efficiency and exergy efficiency.

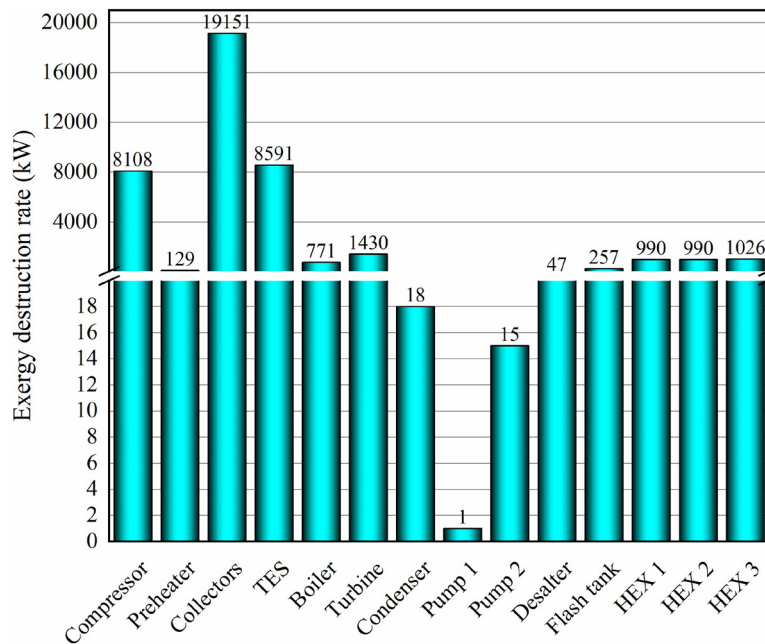


Figure 8: The exergy destruction rate of each component.

singularity in the design and operation of the system. Meanwhile, the non-linear variation in TES performance efficiency stems from the presence of various non-linear factors within the system and the impact of external conditions.

Figure 8 shows the exergy destruction rate of the main components of the system. As depicted in the figure, the solar collectors have the highest ratio followed by the TES tank. This is followed by the compressor, then the turbine and three heat exchangers. In contrast, the preheater, boiler, desalter, flash tank, condenser, and especially the pumps, maintain the lowest exergy destruction rates. This is due to the relatively low mass flow rate of the working fluid considered in the Rankine cycle. As shown in Equation (21), the exergy destruction rate is directly related to the entropy generation, which, in turn, correlates with the difference in operating temperature within the system. Due to the large temperature difference between the temperature of collectors and the temperature of HTF, the solar collectors will have high entropy generation, resulting in high exergy destruction rate. Similarly, in the Rankine cycle, the destruction rate is also smaller due to the smaller temperature difference between the temperature of boiler and the temperature of steam, resulting in low entropy. Therefore, efforts are needed to reduce exergy destruction rates in a cost-effective manner. The main results of the study are summarized in Table 8.

Table 8: Main findings of thermodynamic analysis.

PARAMETER	VALUE
The number of collectors used	259
Land requirement	31339 m ²
Generated thermal energy in solar collectors	28163 kW
CO ₂ reduction	11724 t/y
Refining capacity	441504 t/y
Annual solar heat generation	8250 (MW · h)/y
Storage capacity of TES tan <i>k</i>	270.88 MJ
Heat gain at the first heat exchanger	3205.05 kW
Heat gain at the second heat exchanger	3794.31 kW
Heat gain at the third heat exchanger	4648.65 kW
Waste heat recovery efficiency	31.21%
Solar plant energy efficiency	94.56%
Solar plant exergy efficiency	11.21%
TES tan <i>k</i> energy efficiency	58.12%
TES tan <i>k</i> exergy efficiency	65.31%
Rankine cycle energy efficiency	28.01%
Rankine cycle exergy efficiency	41.59%
Overall energy efficiency	75.99%
Overall exergy efficiency	74.13%
Waste heat recovery efficiency	31.21%

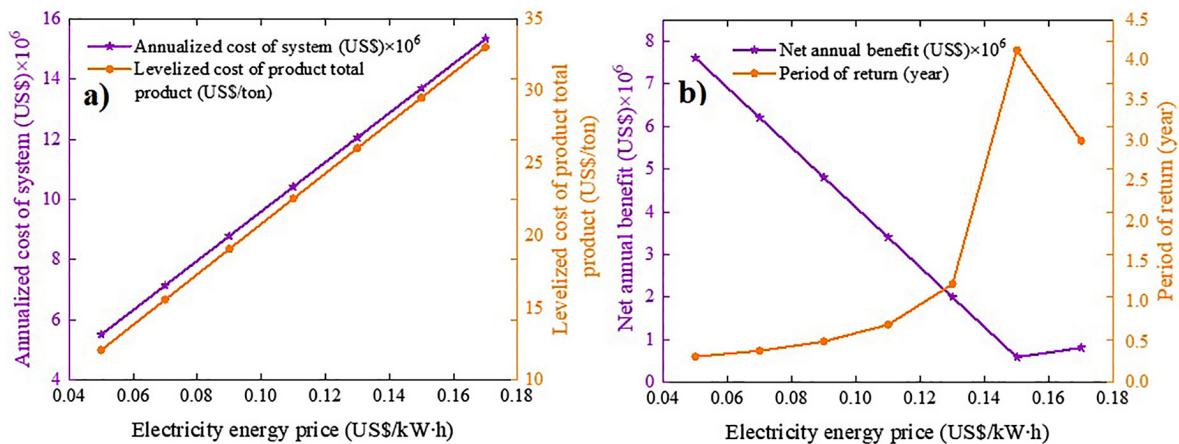


Figure 9: The effect of electricity energy price on (a) annualized cost of system and levelized cost of product, and (b) net annual benefit and period of return.

The variation of the annual cost of the system and the product leveling cost with the electricity price is shown in Figure 9(a). The rise in electricity prices has led to an increase in both the annualized cost of the system and the product leveling cost. This is because the increase in electricity prices first leads to an increase in annual operating costs, which indirectly increases the annualized cost of the system. For product leveling costs, when the annual heating quality of the product remains unchanged, the increase in annualized operating costs will also lead to an increase in this value. Figure 9(b) shows the impact of electricity price on annual net income and return period. As electricity price increases, annual net income first decreases and then increases, while return period first increases and then decreases. Like the analysis in Figure 9(a), the increase in electricity prices has

Table 9: Results of economic analysis of the system.

PARAMETER	UNIT	VALUE
Capital cost	Million US\$	2.215
Crude oil heating price	Million US\$ per year	12.7008
Solar power generation cost	Million US\$ per year	1.187
Summary of product cost	Million US\$ per year	13.888
Prime cost of product	US\$ per ton crude oil	31.334
Net annual benefit	Million US\$ per year	0.591
Annualized cost of system	Million US\$ per year	13.691
Net present value	Million US\$ per year	212.257
Period of return	Year	4.124
Rate of return	Percent	24.252
Insurance cost	US\$ per year	44305.559
Water cost	Million US\$ per year	0.474
Annualized operating cost	Million US\$ per year	13.265

led to an increase in the annual operating costs of the system. Therefore, the annual net income of the system presents a trend of decreasing first, while the return period presents a trend of increasing first. However, when the electricity price is higher than 0.15 US\$/kWh, the annual net income of the system and the return period present an opposite trend. This is because when the electricity price is higher than 0.15 US\$/kWh, the growth rate of the total product cost is faster than the annual operating cost of the system, resulting in an increase in the annual net income of the system and a decrease in the return period. According to Figure 9(b), when the electricity price is around 0.15 US\$/kWh, the return period is less than 4 years, which can prove that the designed solar heating crude oil system structure is reasonable from an economic perspective. For projects with a life of 20 years, a return period of less than 4 years can be used [28]. Table 9 shows the economic analysis results of the system. Related literature has shown that in practical engineering, the investment payback period for solar heating systems is 9.3 years and 7 years, respectively. In theory, the investment payback period in this work has an advantage of 4.124 years, which needs to be put into practice [31].

5. CONCLUSIONS

In this work, a solar cogeneration system for crude oil heating and power generation is proposed. To evaluate its feasibility, this work conducts thermodynamic and economic analysis to evaluate the energy efficiency, exergy efficiency, and economic performance of the overall system. Furthermore, the effect of different system parameters and operating conditions on the performance of the developed system is also investigated. The main concluding observations are summarized as follows:

- (1) The collector provides 28163 kW of energy for the system, and the heat gains of the first, second and third heat exchangers are 3205.05 kW, 3794.31 kW, and 4648.65 kW, respectively. The overall energy efficiency, exergy efficiency and waste heat recovery efficiency reached 75.99%, 74.13% and 31.21%, respectively. Furthermore, the proposed heating system has an annual refining capacity of 441504 tons, which can reduce carbon dioxide emissions by 11724 tons per year.
- (2) Compressor pressure ratio and Rankine cycle fluid flow rate have a significant influence on system performance, and reasonable selection of parameters will greatly help system performance improvement. The components with the largest exergy damage rate in the system are the collector, heat accumulator and compressor, and the pump has the lowest exergy damage rate in the system. Therefore, in order to further improve the system performance, more attention should be paid to the design of the collector, TES tank and compressor to reduce their exergy destruction rate.
- (3) The period of investment return, net annual benefit, and the prime cost of product are 4.124 years, 0.591 million US\$ per year, and 31.334 US\$ per ton of crude oil, respectively. The results of economic analysis highlight the feasibility of the designed system from an economic perspective.

ACKNOWLEDGMENTS

This work was supported by the National Natural Science Foundation of China (No. 52006094), Educational Commission of Liaoning Province of China (LJKMZ20220719, JYTMS20231452). It was also supported by Fushun Revitalization Talents Program (No. FSYC202107007).

REFERENCES

- [1] CHEPELIEV, M., VAN DER MENSBRUGGHE, D., “Global fossil-fuel subsidy reform and Paris Agreement”, *Energy Economics*, v. 85, pp. 104598, 2020. doi: <https://doi.org/10.1016/j.eneco.2019.104598>.
- [2] COZZI, L., GOULD, T., BOUCKART, S., *et al.*, *World energy outlook 2020*, Paris, International Energy Agency, pp. 1–461, 2020.
- [3] HOU, H., DU, Q., HUANG, C., *et al.*, “An oil shale recovery system powered by solar thermal energy”, *Energy*, v. 225, pp. 120096, 2021. doi: <https://doi.org/10.1016/j.energy.2021.120096>.
- [4] HOSSAIN, M.Z., ILLIAS, H.A., “Binary power generation system by utilizing solar energy in Malaysia”, *Ain Shams Engineering Journal*, v. 13, n. 4, pp. 101650, 2022. doi: <http://dx.doi.org/10.1016/j.asej.2021.11.019>.
- [5] VASSILIADES, C., SAVVIDES, A., BUONOMANO, A., “Building integration of active solar energy systems for façades renovation in the urban fabric: effects on the thermal comfort in outdoor public spaces in Naples and Thessaloniki”, *Renewable Energy*, v. 190, pp. 30–47, 2022. doi: <http://dx.doi.org/10.1016/j.renene.2022.03.094>.
- [6] DONG, S., ZHAO, Y., YANG, J., *et al.*, “Solar water recycling of carbonaceous aerogel in open and closed systems for seawater desalination and wastewater purification”, *Chemical Engineering Journal*, v. 431, no. Pt 1, pp. 133824, 2022. doi: <https://doi.org/10.1016/j.cej.2021.133824>.
- [7] WANG, J., O'DONNELL, J., BRANDT, A.R., “Potential solar energy use in the global petroleum sector”, *Energy*, v. 118, pp. 884–892, 2017. doi: <http://dx.doi.org/10.1016/j.energy.2016.10.107>.
- [8] MAHMOUDAN, A., SAMADOF, P., SADEGHZADEH, M., *et al.*, “Thermodynamic and exergoeconomic analyses and performance assessment of a new configuration of a combined cooling and power generation system based on ORC–VCR”, *Journal of Thermal Analysis and Calorimetry*, v. 145, n. 3, pp. 1163–1189, 2021. doi: <https://doi.org/10.1007/s10973-020-10230-y>.
- [9] RAVINDER, K., AVDHESH, K.S., TEWARI, P.C., “Thermal performance and economic analysis of 210 MWe coal-fired power plant”, *Journal of Thermodynamics*, v. 2014, pp. 520183, 2014. doi: <https://doi.org/10.1155/2014/520183>.
- [10] HALABI, M.A., AL-QATTAN, A., AL-OTAIBI, A., “Application of solar energy in the oil industry—Current status and future prospects”, *Renewable & Sustainable Energy Reviews*, v. 43, pp. 296–314, 2015. doi: <http://dx.doi.org/10.1016/j.rser.2014.11.030>.
- [11] IRENA, I., *Global renewables outlook: Energy transformation 2050*, Abu Dhabi, International Renewable Energy Agency, 2020.
- [12] SONG, C., ZHOU, H., GUO, R., *et al.*, “Technology for optimizing flue gas pollutant emission reduction in oil field heating furnace combustion”, *IOP Conference Series: Earth and Environmental Science*, v. 769, n. 2, pp. 022044, 2021. doi: <http://dx.doi.org/10.1088/1755-1315/769/2/022044>.
- [13] KARANIKAS, J.M., PASTOR, G., PENNY, S., “Downhole electric heating of heavy-oil wells”, *CT&F Ciencia, Tecnología y Futuro*, v. 10, n. 2, pp. 61–72, 2020. doi: <http://dx.doi.org/10.29047/01225383.273>.
- [14] SAKTHI, S., MAHENDRAN, S., JAYASUTHAHAR, T., “An effect of nano-SiC with different dielectric mediums on AZ61/7.5% B4C nanocomposites studied through electrical discharge machining and Taguchi based complex proportional assessment method”, *Matéria (Rio de Janeiro)*, v. 28, n. 2, pp. 20230058, 2023. doi: <https://doi.org/10.1590/1517-7076-RMAT-2023-0058>.
- [15] XU, L.H., QIANG, W.F., DONG, Z., *et al.*, “Experimental investigation of cost-effective ZnO nanofluids based spectral splitting CPV/T system”, *Energy*, v. 194, pp. 116913, 2020. doi: <https://doi.org/10.1016/j.energy.2020.116913>.
- [16] GUPTA, K., ETHAKOTA, M., PAYYANAD, S., “Integrate solar/thermal energy in oil and gas processing”, *Hydrocarbon Processing*, v. 97, n. 1, pp. 35–42x-x, 2018.
- [17] SHUAI, Y., XIA, X.-L., TAN, H.-P., “Radiation performance of dish solar concentrator/cavity receiver systems”, *Solar Energy*, v. 82, n. 1, pp. 13–21, 2008. doi: <http://dx.doi.org/10.1016/j.solener.2007.06.005>.

- [18] NUNES, V.F., LIMA, F.M., TEIXEIRA, E.S., *et al.*, “Effects of tin on the performance of ZnO photoanode for DSSC”, *Matéria (Rio de Janeiro)*, v. 26, n. 4, pp. e13112, 2021. doi: <http://dx.doi.org/10.1590/s1517-707620210004.1312>.
- [19] CHENG, Z., HAN, H., WANG, F., *et al.*, “Efficient radiative cooling coating with biomimetic human skin wrinkle structure”, *Nano Energy*, v. 89, n. Pt. A, pp. 106377, 2021. doi: <https://doi.org/10.1016/j.nanoen.2021.106377>.
- [20] WU, S.Y., XIAO, L., CAO, Y., *et al.*, “A parabolic dish/AMTEC solar thermal power system and its performance evaluation”. *Applied Energy*, v. 87, n. 2, pp. 452–462, 2010. doi: <https://doi.org/10.1016/j.apenergy.2009.08.041>.
- [21] MORADI, M., MEHRPOOYA, M., “Optimal design and economic analysis of a hybrid solid oxide fuel cell and parabolic solar dish collector, combined cooling, heating and power (CCHP) system used for a large commercial tower”, *Energy*, v. 130, pp. 530–543, 2017. doi: <http://dx.doi.org/10.1016/j.energy.2017.05.001>.
- [22] REYHANI, H.A., MERATIZAMAN, M., EBRAHIMI, A., *et al.*, “Thermodynamic and economic optimization of SOFC-GT and its cogeneration opportunities using generated syngas from heavy fuel oil gasification”, *Energy*, v. 107, pp. 141–164, 2016. doi: <https://doi.org/10.1016/j.energy.2016.04.010>.
- [23] GHORBANI, B., MEHRPOOYA, M., SHIMMOHAMMADI, R., *et al.*, “A comprehensive approach toward utilizing mixed refrigerant and absorption refrigeration systems in an integrated cryogenic refrigeration process”, *Journal of Cleaner Production*, v. 179, pp. 495–514, 2018. doi: <https://doi.org/10.1016/j.jclepro.2018.01.109>.
- [24] GALANTI, L., MASSARDO, A.F., “Micro gas turbine thermodynamic and economic analysis up to 500 kWe size”, *Applied Energy*, v. 88, n. 12, pp. 4795–4802, 2011. doi: <http://dx.doi.org/10.1016/j.apenergy.2011.06.022>.
- [25] MANESH, M.H.K., GHALAMI, H., AMIDPOUR, M., *et al.*, “Optimal coupling of site utility steam network with MED-RO desalination through total site analysis and exergoeconomic optimization”, *Desalination*, v. 316, pp. 42–52, 2013. doi: <https://doi.org/10.1016/j.desal.2013.01.022>.
- [26] BENATO, A., “Performance and cost evaluation of an innovative Pumped Thermal Electricity Storage power system”, *Energy*, v. 138, pp. 419–436, 2017. doi: <http://dx.doi.org/10.1016/j.energy.2017.07.066>.
- [27] GIBSON, C.A., MEYBODI, M.A., BEHNIA, M., “Optimization and selection of a steam turbine for a large scale industrial CHP (combined heat and power) system under Australia’s carbon price”, *Energy*, v. 61, pp. 291–307, 2013. doi: <http://dx.doi.org/10.1016/j.energy.2013.08.045>.
- [28] GHORBANI, B., SHIRMOHAMMADI, R., MEHRPOOYA, M., “A novel energy efficient LNG/NGL recovery process using absorption and mixed refrigerant refrigeration cycles–Economic and exergy analyses”, *Applied Thermal Engineering*, v. 132, pp. 283–295, 2018. doi: <http://dx.doi.org/10.1016/j.applthermaleng.2017.12.099>.
- [29] GHORBANI, B., HAMED, M.H., AMIDPOUR, M., *et al.*, “Implementing absorption refrigeration cycle in lieu of DMR and C3MR cycles in the integrated NGL, LNG and NRU unit”, *International Journal of Refrigeration*, v. 77, pp. 20–38, 2017. doi: <http://dx.doi.org/10.1016/j.ijrefrig.2017.02.030>.
- [30] KARAGIANNIS, I.C., SOLDATOS, P.G., “Water desalination cost literature: review and assessment”, *Desalination*, v. 223, n. 1–3, pp. 448–456, 2008. doi: <http://dx.doi.org/10.1016/j.desal.2007.02.071>.
- [31] ABD EL RAHMAN, A.M., NAFEY, A.S., HASSANIEN, M.H.M., “Application of solar energy heating system in some oil industry units and its economy”, *Journal of Fundamental Renewable Energy Applications*, v. 7, n. 4, pp. 1000233, 2017. doi: <http://dx.doi.org/10.4172/2090-4541.1000233>.